Catalysis Today 160 (2011) 96–102

Contents lists available at ScienceDirect

Catalysis Today

journal homepage: www.elsevier.com/locate/cattod

Structural analysis of palladium-decorated gold nanoparticles as colloidal bimetallic catalysts

Yu-Lun Fang[a], Jeffrey T. Miller[b], Neng Guo[b], Kimberly N. Heck[a], Pedro J.J. Alvarez[c,d], Michael S. Wong[a,d,e,*]

[a] Department of Chemical and Biomolecular Engineering, Rice University, 6100 S. Main Street, Houston, TX 77005, USA
[b] Chemical Sciences and Engineering Division, Argonne National Laboratory, 9700 S. Cass Avenue, Argonne, IL 60439, USA
[c] Department of Civil and Environmental Engineering, Rice University, USA
[d] Center of Biological and Environmental Nanotechnology, Rice University, USA
[e] Department of Chemistry, Rice University, USA

ARTICLE INFO

Article history:
Available online 20 September 2010

Keywords:
Colloidal bimetallic nanoparticle catalyst
Palladium
Gold
XAS
XANES
EXAFS
Hydrodechlorination
Trichloroethene

ABSTRACT

Bimetallic palladium-decorated gold nanoparticle (Pd/Au NP) catalysts are significantly more active than palladium-only catalysts, but the mechanism for enhancement is not completely clear for most reactions, like the aqueous-phase hydrodechlorination of trichloroethene. In this study, we conducted X-ray absorption spectroscopy on carbon-supported Pd/Au NPs to obtain information about the local atomic environment (i.e., oxidation states, coordination numbers, and bond distances) of the two metals under different treatment conditions. The as-synthesized NPs were confirmed to have a Pd-shell/Au-core nanostructure, in which the Pd was found as surface ensembles. Upon exposure to room temperature in air, a portion of the Pd, but not the Au, was oxidized. In comparison, nearly the entire surface of monometallic Pd NPs was oxidized, suggesting that Au in Pd/Au NPs imparts oxidation resistance to Pd atoms. The surface Pd was found randomly distributed, presumably as a PdAu surface alloy, after reduction at 300 °C. X-ray absorption spectroscopy provides direct evidence for the Pd-shell/Au-core structure of Pd/Au NPs, and suggests that metallic Pd in the Pd/Au NPs is a source for higher catalytic activity for aqueous-phase trichloroethene hydrodechlorination.

1. Introduction

Structural characterization of catalysts provides a key to understanding the observed catalytic properties with regard to their surface active sites [1–3]. For supported bimetallic catalysts, it is generally accepted that catalysis performance, activity, selectivity, and/or stability, can be enhanced compared to that of the supported monometallic catalysts due to the synergistic combination of the two metals (in the nominal form of bimetallic nanoparticles (NPs) on the support surface) [4–7]. Three common explanations have been proposed to account for the catalytic enhancement [8–16]: (1) the geometric effect, in which atomic ensembles act as active sites; (2) the electronic effect, in which interaction among surrounding atoms gives rise to electron density dislocation; and (3) the bifunctional effect, in which each metal promotes a different step of the surface reaction. In principle, these proposed mechanisms should also apply to unsupported bimetallic NPs, but this class of catalysts has been much less studied [1–3].

Many spectroscopic and microscopic methods, such as electron microscopy, scanning probe microscopy, X-ray diffraction, energy disperse X-ray microanalysis, ultraviolet-visible, infrared, surface-enhanced Raman, X-ray photoelectron, Mössbauer, and nuclear magnetic resonance, have been used to determine the structure of bimetallic NPs [1–3]. X-ray absorption spectroscopy (XAS) is a powerful technique to acquire detailed structural and electronic information on metallic NPs [17–19]. There are two regions of interest in an X-ray absorption spectrum: the X-ray absorption near-edge structure (XANES) and extended X-ray absorption fine structure (EXAFS) regions. When the incident photon energy is near the absorption edge of a chemical element, the XANES region can provide information about oxidation state, electron distribution, and site symmetry of the absorbing atom. The EXAFS region, where oscillatory absorption occurs at higher incident photon energy due to interference of the ejected photoelectron with electron waves back-scattered from surrounding atoms, provides structural information about neighboring atoms to the absorbing one. XAS, especially in the EXAFS region, has been applied for characterization of bimetallic nanoparticles for decades. Sin-

* Corresponding author at: Department of Chemical and Biomolecular Engineering, Rice University, 6100 S. Main Street, Houston, TX 77005, USA.
Tel.: +1 713 348 3511; fax: +1 713 348 5478.
E-mail address: mswong@rice.edu (M.S. Wong).

0920-5861/$ – see front matter © 2010 Elsevier B.V. All rights reserved.
doi:10.1016/j.cattod.2010.08.010

$$ClHC{=}CCl_2 + 4\ H_2 \rightarrow H_3C\text{-}CH_3 + 3\ HCl$$

Scheme 1. TCE HDC overall reaction.

felt and co-workers conducted comprehensive XAS studies on various supported bimetallic catalysts prepared through conventional metal salt impregnation techniques [20–24]. Toshima and co-workers as well as other researchers performed the early work on XAS of bimetallic NPs in colloidal (i.e., unsupported) and immobilized (i.e., supported) forms [25–36]. There has been increasing use of XAS to characterize bimetallic NPs in recent years, revealing several possibilities for the two metals to be distributed within a NP, for example, alloy [34,37–41], core–shell [26,37,39–46], cluster-in-cluster [28,47,48], and multi-shell structures [2,49].

Through this study, we analyzed the nanostructure of palladium-decorated gold NPs (abbreviated here as Pd-on-Au NPs or Pd/Au NPs) prepared in aqueous suspension. We previously showed that Pd/Au NPs were at least one order of magnitude more active than Pd NPs, Pd-on-alumina (Pd/Al_2O_3), and Pd black on a per-Pd-atom basis for the room-temperature, aqueous-phase hydrodechlorination (HDC) of trichloroethene (TCE) [50–54], which converts TCE to ethane as shown in Scheme 1.

Pd/Au and Pd catalysts both exhibited >97% selectivity to ethane for TCE HDC reactions [51]. The presumptive nanostructure of the catalyst was a one-atom-thick Pd shell on 4-nm Au NPs, with maximum activity found for NPs partially covered by Pd atoms (with ~60–70% Pd surface coverage). Based on batch kinetic studies and characterization results, we proposed that geometric and electric effects could explain the catalytic enhancement [51]. Through careful XAS measurement and analysis of Pd/Au NPs with 60% Pd coverage and comparison with Au NPs and Pd NPs, we confirmed the core-shell bimetallic structure in this work. By studying the effect of heat treatment, we found the Pd shell to be in the form of Pd ensembles on the Au NP surface. At ambient temperature, a portion of the Pd surface atoms remained metallic in the Pd/Au NPs while most of the surface atoms were oxidized in Pd NPs, suggesting that zero-valent Pd contributes to the higher catalytic activity of Pd/Au NPs.

2. Experimental

2.1. Preparation of NP catalysts

Nanoparticles, including Au NPs, Pd/Au NPs, and Pd NPs, were prepared as previously reported [51]. For Au NPs, a gold salt solution was prepared by diluting 1 mL $HAuCl_4$ solution (0.236 M; $AuCl_3$ 99.99%, Sigma–Aldrich; $AuCl_3$ was dissolved in water at room temperature) in 80 mL Nanopure water (>18.0 MΩ-cm, Barnstead NANOpure Diamond). A second solution was prepared by dissolving 0.04 g trisodium citrate (>99.5%, Fisher), 0.05 g tannic acid (>99.5%, Sigma–Aldrich), and 0.018 g potassium carbonate (>99.5%, Sigma–Aldrich) in 20 mL Nanopure water. Both solutions were heated to 60 °C and kept at 60 °C for at least 5 min. The second solution was then added to the gold salt solution. The overall fluid was kept stirring vigorously, and was heated to boil for 20 min before the heat source was removed. The color of the heated overall fluid changed with time—from light yellow to reddish, brown, and finally dark brown. Au NPs in the final fluid were about 4-nm in diameter according to transmission electron microscopy (TEM), and the concentration was calculated to be 1.07×10^{14} NP/mL, assuming 100% reduction of Au salts.

Pd/Au NPs were prepared with Au NPs modeled as "magic clusters" with 7 complete shells of gold atoms and an additional Pd shell of different coverages [51]. The magic cluster model describes atom stacking by the way of a central atom surrounded with closed shells of identical atoms, which is the same arrangement as the face-centered cubic (FCC) system [51,55–57]. In this work, Pd/Au NPs with a 60% Pd surface coverage (= 0.6 monolayer = 0.6 ML) were chosen as a representative sample because of the highest activity. To prepare 0.6 ML Pd/Au NPs, 57 μL H_2PdCl_4 solution (0.00240 M), which was prepared by dissolving $PdCl_2$ (99.99%, Sigma–Aldrich) in 0.005 M $HCl_{(aq)}$ with moderate stirring, was mixed with 2 mL as-synthesized Au NP suspension (1.07×10^{14} NP/mL). The fluid was then bubbled with hydrogen gas (99.99%, Matheson) for 2 min, and left to age overnight at room temperature (RT, 22 ± 2 °C). Hydrogen gas served as a reducing agent for Pd salts; as we previously reported [51], Pd(0) atoms would be deposited on the surface of Au NPs rather than forming Pd particles because the activation energy for heterogeneous nucleation is less than that for homogeneous nucleation [58].

For Pd NPs, the preparation was the same as Au NPs, except that the gold salt solution was replaced by the palladium salt solution, which was prepared by diluting 12 mL H_2PdCl_4 solution (0.00240 M) in 68 mL Nanopure water. The color of the heated overall fluid also changed with time, from light yellow to brown. Pd NPs in the final fluid were about 4-nm in diameter according to TEM, and the concentration was calculated to be 1.22×10^{14} NP/mL, assuming 100% reduction of Pd salts.

2.2. Catalyst characterization

2.2.1. Transmission electron microscopy (TEM)

Size distributions of the NP samples were determined by analysis of imaging with a JEOL 2010 transmission electron microscope. TEM samples were prepared by depositing NP suspension on a 200-mesh carbon/formvar TEM grid and air-dried at RT. Size distribution measurements were conducted with the ImageJ program [59]; 150 particles were counted for each sample.

2.2.2. X-ray absorption spectroscopy (XAS)

NPs were immobilized on carbon powder for XAS experiments. 0.2 g carbon powder (Vulcan XC-72, Cabot) was dispersed in 5 mL isopropanol (99.9%, Fisher) under ultrasonication for 5 min. A given NP suspension (Au NPs, 0.6 ML Pd/Au NPs, or Pd NPs) was added to the carbon powder dispersion, and resulting mixture was ultrasonicated for 30 min and then stirred for 2 h. Afterward, the mixture was freeze-dried at −50 °C with a vacuum pressure 0.066 mbar (Labconco FreeZone 4.5 L console freeze dry system) to generate NP-containing carbon powders (NP/C). This low-temperature freeze-drying process for NP immobilization increased the metal loadings in the final solid, allowing for better XAS signal-to-noise ratios without heat effects that would damage the bimetallic nanostructure. The final solid compositions for Au NP/C, 0.6 ML Pd/Au NP/C, and Pd NP/C were respectively 5 wt.% Au, 5 wt.% Au with 0.75 wt.% Pd, and 1 wt.% Pd, estimated from mass balance with the assumption that all Pd and Au contents in the system were deposited on the carbon support.

X-ray absorption measurements were carried out on the insertion-device beamline 10-ID-B of the Materials Research Collaborative Access Team (MRCAT) at the Advanced Photon Source at Argonne National Laboratory. A cryogenically cooled double-crystal Si (1 1 1) monochromator was used in conjunction with an uncoated glass mirror to minimize the presence of harmonics. The monochromator was scanned continuously during the measurements with data points integrated over 0.5 eV for 0.07 s per data point. Measurements were made in transmission mode with the ionization chambers optimized for the maximum current with linear response (~10^{10} photons detected per second) using a mixture of nitrogen and helium in the incident X-ray

detector and a mixture of ~20% argon in nitrogen in the transmission X-ray detector. A gold or palladium foil spectrum was acquired simultaneously with each measurement for energy calibration.

The NP/C samples were pressed into a cylindrical holder with a thickness chosen to give a total absorbance (μx) at the Au L_{III} (11.918 keV) and Pd K (24.350 keV) edges of ca. 2.0, and an edge step ($\Delta\mu x$) of ca. 0.5. Samples were analyzed as-prepared in air, He, or H_2 at RT. Separate samples were reduced at 100 °C, 250 °C, or 300 °C for 30 min in 4% H_2/He followed by He purge at 200 °C in a continuous-flow reactor cell (glass tube, length 18 in., diameter 0.75 in.) fitted at both ends with polyimide windows and stainless steel valves to isolate the reactor from the atmosphere. Purging of the reduced catalysts in He at 200 °C was sufficient to decompose any Pd–H that might have been present and to desorb chemisorbed H_2 molecules. All spectra were obtained at RT.

Experimental phase shifts and back-scattering amplitudes were obtained from reference compounds: $Pd(NH_3)_4(NO_3)_2$ (Aldrich) for Pd–O, Pd foil for Pd–Pd, and Au foil for Au–Au. Experimen-

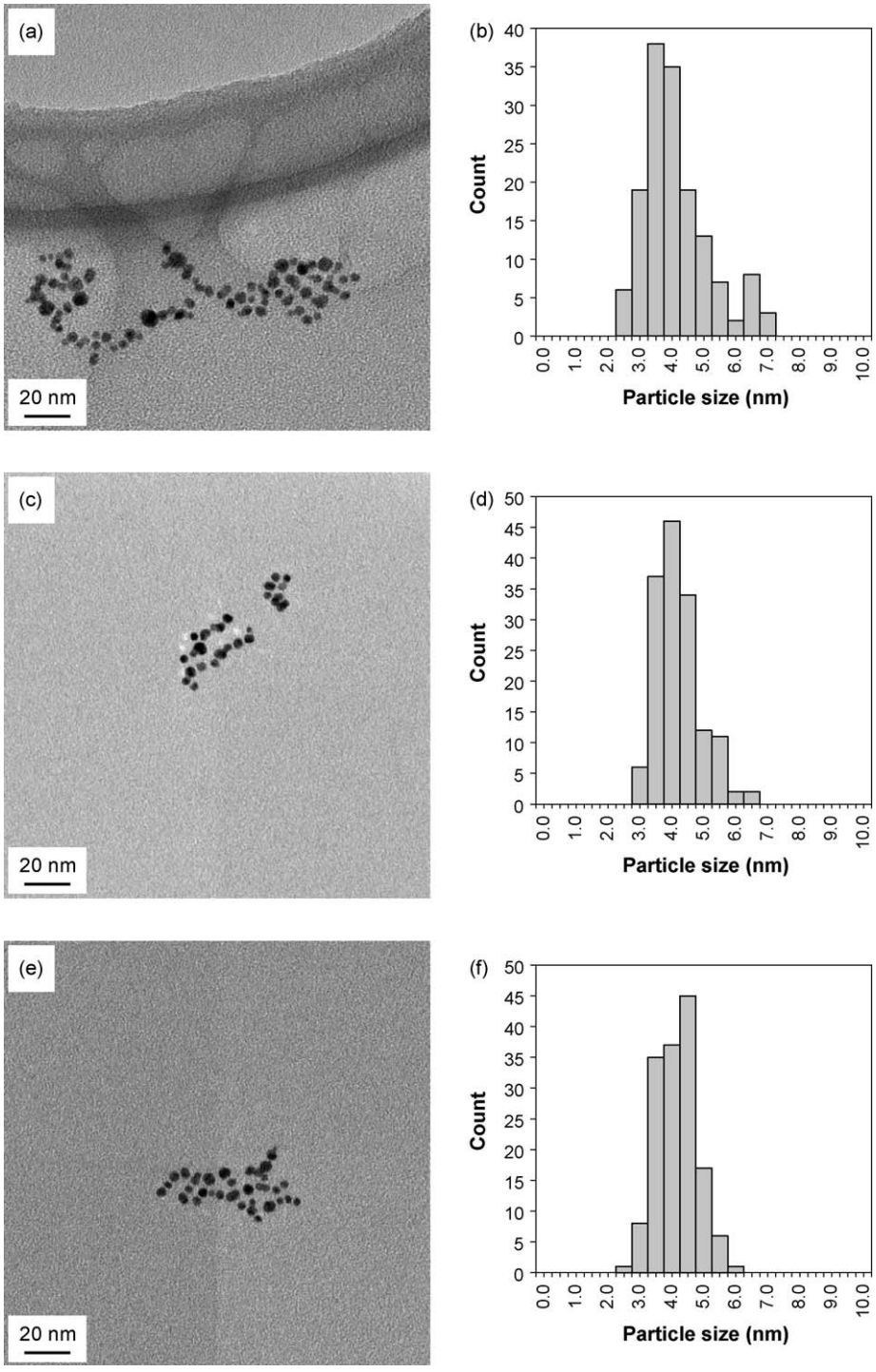

Fig. 1. Representative TEM images and particle size histograms of (a and b) Au NPs, (c and d) 0.6 ML Pd/Au NPs, and (e and f) Pd NPs. A population of 150 nanoparticles was analyzed for each NP sample.

tal data of Pd and Au foil were used to determine the best fit of Debye–Waller factors (DWF) and amplitude reduction factors (S_o) for phase shifts and back-scattering amplitudes in the FEFF fitting [60]. Along with the bond distance for Au and Pd foil, these values were used for determining the Au–Pd and Pd–Au FEFF phase shifts and back-scattering amplitudes. Standard procedures based on the WINXAS97 software [60] were used to extract the data [61]. The coordination parameters were obtained by a least-square fit in *k*- and *R*-space of the nearest-neighbor, k^2-weighted Fourier transform (FT) data (*k*: photoelectron wave number). The data fitted equally well with both k^1 and k^3 weightings. For the bimetallic Pd/Au sample, the EXAFS fitting was verified that, within error, the data from both Pd and Au edges led to the same bond distances, the same DWF's, and self-consistent coordination numbers for Pd–Au and Au–Pd bonds [62].

2.3. Trichloroethene hydrodechlorination (TCE HDC) rate determination

NP suspensions were tested in batch reactors for TCE HDC reactions, performed according to the previous studies [51]. Nanopure water and a magnetic stir bar were sealed in a screw-cap bottle (250 mL, Alltech) with PTFE-sealed threads and a PTFE-silicone septum. The initial water volume was controlled to make the final liquid volume 173 mL after addition of the nanoparticle suspension. Hydrogen gas was bubbled into the bottle for 15 min to displace dissolved oxygen and to fill the headspace with a hydrogen atmosphere (1 atm). Then 7 μL TCE (99.5%, Sigma–Aldrich) and 0.2 μL pentane (99.7%, Burdick and Jackson), as the internal standard, were injected into the sealed bottle. The overall solution was stirred for at least 3 h to reach equilibrium. The initial TCE concentration in water was 50.9 ppm, far below the saturation concentration of 1200 ppm in water at 25 °C. Afterward, at time $t = 0$, NP suspension (Au NPs, Pd/Au NPs, or Pd NPs) was injected into the reaction bottle stirred at 600 rpm. The reaction was monitored through headspace gas chromatography (GC) using an Agilent Technologies 6890N GC with a flame ionization detector (FID) and a 60/80 Carbopack B/1% SP-1000 packed column (Supelco 12487, Sigma–Aldrich). Gas samples were taken from the headspace (gas phase) of the reactor, and then injected into GC to determine quantities of TCE and other compounds (>97% selectivity to ethane [51]). Reaction rates were determined from change of TCE concentrations in the headspace. All the reactions were performed at room temperature; reactions were performed with NP suspensions and not with either NP/C or heat-treated NP/C samples.

3. Results and discussion

3.1. TEM analysis

TEM images provided particle size information for the monometallic Au, 0.6 ML Pd/Au, and monometallic Pd NPs (Fig. 1). The mean particle sizes (and relative standard deviations) were similar and estimated to be 4.1 nm (24%), 4.2 nm (17%), and 4.1 nm (15%) for Au NPs, 0.6 ML Pd/Au NPs, and Pd NPs, respectively.

3.2. XAS analysis

The XANES spectra of Au NP/C at the Au edge in air, He, or H_2 (Fig. 2) were almost identical to that of Au foil (reference compound for Au–Au bond), indicating that the Au NPs were metallic with little oxidized Au. The k^2-weighted Fourier transform of EXAFS data for Au NP/C (Fig. 3) also gave no evidence for the presence of Au–O bonds (bond distance of 2.03 Å). The XANES spectra did not change after RT treatment in air, He, or H_2 or after reduction at 250 °C.

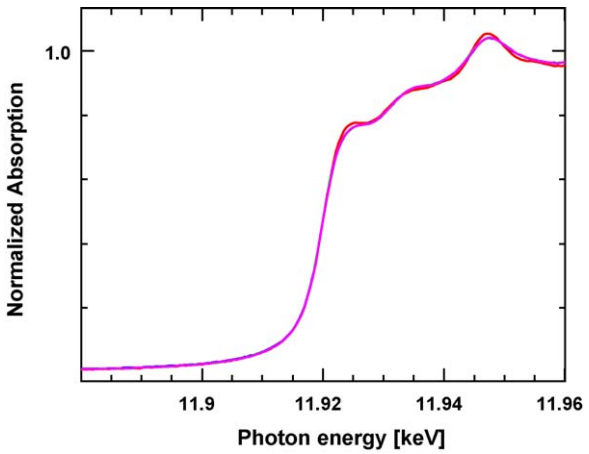

Fig. 2. XANES spectra of Au foil (red) at RT and Au NP/C in air (blue), He (pink), and H_2 (green) at RT. (For interpretation of the references to color in this figure legend, the reader is referred to the web version of this article.)

Table 1 shows the results of EXAFS fitting. The Au–Au coordination number (N_{Au-Au}) of Au NP/C was about 10, and was estimated to correspond to approximately 5.5 nm particles [63]. This particle size was slightly larger than the 4.1 nm average diameter measured from TEM, which might be attributed to EXAFS being more sensitive to larger particles. The bond distance in the Au NPs was 2.86 Å, slightly less than that of Au foil (2.88 Å), which is typical of NPs. The Au–Au bond distance and coordination number did not change after RT treatment in air, He, or H_2 or after reduction at 250 °C (Table 1).

The EXAFS of Pd NPs indicated partial oxidation in air at RT and in H_2 up to 100 °C. Fits of the oxidized catalysts gave a Pd–Pd coordination number ($N_{Pd-Pd} = 8.1$) at a bond distance $R = 2.79$ Å and a Pd–O coordination number ($N_{Pd-O} = 1.3$) at $R = 2.05$ Å. Since PdO has $N_{Pd-O} = 4$, one can estimate the oxidized fraction from the coordination number. Approximately, one-third of the Pd atoms in a Pd NP were oxidized in air at RT, i.e., $1.3/4 = 0.33$, which is similar to the estimated dispersion of about 0.27 (calculated from dispersion $D = c/d$ (*c* is a constant 1.1 for Pd; *d* is the average particle size 4.1 nm from TEM)) [64,65]. These values suggested that nearly all of the surface Pd atoms were oxidized in the monometallic Pd NPs.

Upon reduction at 300 °C, the Pd NPs were fully reduced and the estimated size from $N_{Pd-Pd} = 9.3$ was 4.4 nm, in good agreement with the TEM-derived value of 4.1 nm. The Pd–Pd bond distance

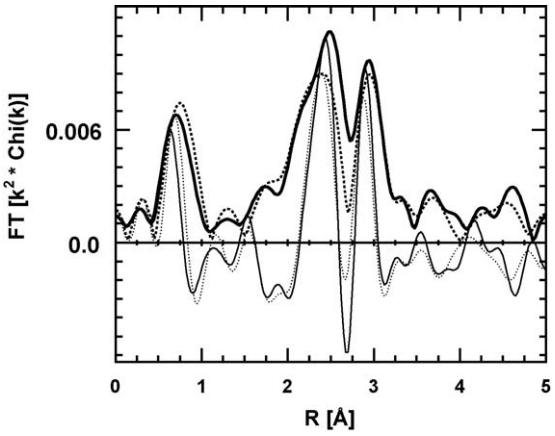

Fig. 3. Fourier transform (k^2 weighted, $\Delta k = 2.6$–12.6 Å^{-1}) of Au L_{III} edge EXAFS data for Au NP/C and 0.6 ML Pd/Au NP/C, both after reduction at 250 °C: magnitude (solid thick) and imaginary components (solid thin) for Au NP/C; magnitude (dotted thick) and imaginary components (dotted thin) for Pd/Au NP/C (Δk: data length of *k* used for fitting).

Table 1
EXAFS fit parameters (N: coordination number; R: bond distance; DWF: Debye–Waller factor; E_0: threshold absorption edge energy).

Sample	Edge	Treatment	Scattering path	N (±10%)	R (Å) (±0.02 Å)	DWF ($\times 10^3$ Å^2)	E_0 (eV)
Au NP/C	Au	Air RT	Au–Au	10.2	2.86	1.0	−3.8
	Au	He RT	Au–Au	10.2	2.86	1.0	−3.7
	Au	H_2 RT	Au–Au	10.2	2.86	1.0	−3.8
	Au	H_2 100 °C	Au–Au	9.8	2.86	1.0	−3.9
	Au	H_2 250 °C	Au–Au	10.2	2.86	1.0	−3.7
Pd NP/C	Pd	Air RT	Pd–Pd	8.1	2.79	2.5	2.8
			Pd–O	1.3	2.05	2.0	1.5
	Pd	H_2 100 °C	Pd–Pd	7.4	2.81	2.5	2.1
			Pd–O	1.2	2.03	2.0	0.3
	Pd	H_2 300 °C	Pd–Pd	9.3	2.80	2.5	1.9
0.6 ML Pd/Au NP/C	Au	Air RT	Au–Au	9.7	2.85	1.0	2.4
			Au–Pd	1.5	2.80	1.0	3.0
	Au	He RT	Au–Au	9.8	2.85	1.0	2.3
			Au–Pd	1.3	2.80	1.0	3.6
	Au	H_2 RT	Au–Au	9.7	2.85	1.0	2.2
			Au–Pd	1.3	2.81	1.0	4.0
	Au	H_2 100 °C	Au–Au	9.6	2.84	1.0	2.2
			Au–Pd	1.3	2.79	1.0	3.9
	Au	H_2 250 °C	Au–Au	9.3	2.85	1.0	2.8
			Au–Pd	1.6	2.83	1.0	4.8
	Pd	Air RT	Pd–Pd	3.3	2.78	1.0	−3.0
			Pd–O	0.9	2.04	1.0	1.5
			Pd–Au	3.8	2.80	1.0	−2.1
	Pd	H_2 RT	Pd–Pd	2.8	2.77	1.0	−4.4
			Pd–O	0.6	2.04	1.0	2.0
			Pd–Au	4.2	2.78	1.0	−2.6
	Pd	H_2 100 °C	Pd–Pd	3.3	2.78	1.0	−4.0
			Pd–O	0.8	2.04	1.0	1.9
			Pd–Au	4.0	2.80	1.0	−1.8
	Pd	H_2 300 °C	Pd–Pd	2.0	2.76	1.0	−3.7
			Pd–Au	6.9	2.79	1.0	−3.2

was 2.80 Å, which was larger than that in Pd foil (e.g., 2.75 Å), and similar to that in Pd–H [66]. These spectra were obtained in He after H_2 desorption at 200 °C without a change in the bond distance. Under the same conditions, supported Pd–H prepared by conventional methods is not stable, decomposing to metallic Pd with a bond distance of 2.75 Å [66]. The reason for these differences is not understood.

At the Au edge for the Pd/Au NPs, $N_{Au–Au}$ was 9.7 at R = 2.85 Å, which was very similar to that in the monometallic Au NPs, consistent with the Au core of Pd/Au NPs being similarly sized to monometallic Au NPs. Unlike the Au NPs, however, the EXAFS indicated the presence of a second scatter, i.e., from Au–Pd with $N_{Au–Pd}$ = 1.3 at 2.80 Å. There was negligible difference in the Au XANES or EXAFS for the 0.6 ML Pd/Au NP/C structure after contacting with air, He, or H_2 at RT (Table 1). However, upon reduction at 250 °C, there was a slight increase in the Au–Pd coordination number to 1.6. There was no evidence of oxidized Au in the Pd/Au NPs.

EXAFS of the Pd edge for 0.6 ML Pd/Au NP/C in air at RT and in H_2 up to 100 °C showed a significant peak near 1.5 Å (the uncorrected distance for Pd–O bond) and metallic peaks between 1.8 and 3.0 Å (Fig. 4). The EXAFS fits indicated that Pd has three coordination environments: metallic Pd ($N_{Pd–Pd}$ = 3.3 at 2.78 Å), metallic Au ($N_{Pd–Au}$ = 4.0 at 2.80 Å), and oxidized Pd^{2+} ($N_{Pd–O}$ = 0.8 at 2.04 Å) (Table 1). Within the error of the EXAFS measurements, the bond distances of Au–Pd ($R_{Au–Pd}$) and Pd–Au ($R_{Pd–Au}$) were identical, ca. 2.80 Å.

From the Pd–O coordination numbers, the fraction of oxidized atoms in the 0.6 ML Pd/Au NPs was estimated to be about 20% (~0.8/4.0) in air or after treatment in H_2 at 100 °C. Assuming nearly all the Pd atoms were located on the Au NP surface as Pd surface atoms, then most of the Pd atoms (~80%) were in the metallic form. Reduction at 300 °C led to complete reduction of Pd and an increase in the Pd–Au coordination number to 6.9, but a decrease in the Pd–Pd coordination number to 2.0.

A more complete analysis of metal coordination numbers provided insights into the Au and Pd distributions in the Pd/Au NPs. For the sample analyzed after treatment in air at RT, $N_{Au–Au}$ = 9.7 and $N_{Au–Pd}$ = 1.5, with the sum as the total Au coordination number of 11.2. The elemental composition was 5 wt.% Au and 0.75 wt.% Pd. At RT in air or H_2 at 100 °C, 80% (or 0.6 wt.% Pd) was metallic. The molar composition of the reduced metal was thus calculated as 82% and 18% for Au and Pd, respectively. If the Pd/Au NPs had a random, uniform distribution of Pd and Au atoms, the coordination number of Au with other Au atoms $N_{Au–Au,bulk}$ would be 9.2 (= 11.2 × 82%),

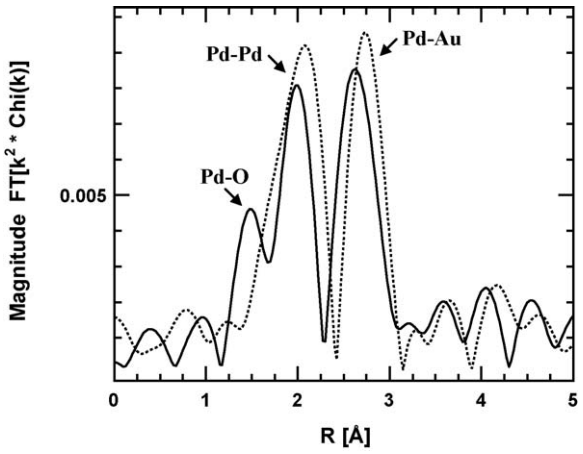

Fig. 4. Fourier transform magnitude components (k^2 weighted, Δk = 2.8–10.5 Å^{-1}) of Pd K edge EXAFS data for 0.6 ML Pd/Au NP/C: in air at RT (solid line), after reduced in H_2 at 300 °C (dotted line).

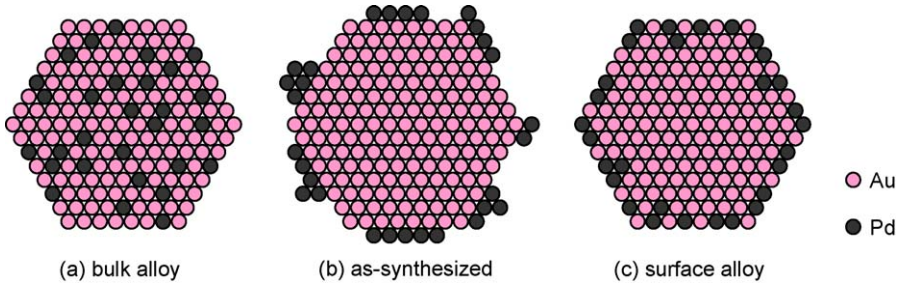

Fig. 5. Idealized cross-sections of (a) a PdAu alloyed NP and core–shell nanostructures of a Pd/Au NP (b) in the as-synthesized form and (c) after reduction in H_2 at 300 °C.

Table 2
Results of catalytic testing for nanoparticle catalysts in aqueous-phase trichloroethene hydrodechlorination (initial $[TCE]_{(aq)}$ = 50.9 ppm, H_2 saturated in water and filled in the headspace (1 atm), stir rate 600 rpm, room temperature 22 ± 2 °C).

Nanoparticle catalysts tested	Pd weight loading (wt.%)	Estimated Pd dispersion (% surface Pd atoms)	Calculated amount of surface Pd charged (nmol)	Initial TOF (mol-TCE/mol-Pd_{surf}/s)
Au NPs	0	n/a	0	0
0.6 ML Pd/Au NPs	12.8	100[a]	60	1.44
Pd NPs	100	27[b]	47	0.15

[a] Pd atoms assumed to be fully accessible on Au NP surface.
[b] Calculated from dispersion $D = c/d$ (c is a constant 1.1 for Pd; d is the average particle size 4.1 nm from TEM) [64,65].

and the coordination number of Au with other Pd atoms $N_{Au-Pd,bulk}$ would be 2.0 (= 11.2 × 18%). Since the measured N_{Au-Au} was greater than $N_{Au-Au,bulk}$ and the measured N_{Au-Pd} was less than $N_{Au-Pd,bulk}$, the Pd/Au NPs were concluded to have a Au-rich core (and a Pd-rich surface). The total absence of a small amount of Pd atoms within the Au core could not be ascertained.

From the Pd edge, N_{Pd-Au} = 3.8 and N_{Pd-Pd} = 3.3, giving a total Pd coordination number of 7.1. For a NP of Pd–Au uniform composition, the coordination number of Pd with Au atoms $N_{Pd-Au,bulk}$ would be 5.8 (= 7.1 × 82%) and the coordination number of Pd with other Pd atoms $N_{Pd-Pd,bulk}$ would be 1.3 (= 7.1 × 18%) (Fig. 5a). Since the measured N_{Pd-Au} was less than $N_{Pd-Au,bulk}$ and the measured N_{Pd-Pd} was greater than $N_{Pd-Pd,bulk}$, the NPs have a Pd-rich surface (Fig. 5b).

All the oxidized Pd atoms in the carbon-supported Pd/Au NPs were reduced in H_2 at 300 °C. The metallic composition was recalculated to be 78% and 22% for Au and Pd, respectively. The total Au coordination number was 10.9, but the total Pd coordination number increased from 7.1 to 8.9. The coordination numbers for a NP of PdAu bulk composition were calculated as $N_{Au-Au,bulk}$ = 8.5, $N_{Au-Pd,bulk}$ = 2.4, $N_{Pd-Au,bulk}$ = 6.9, and $N_{Pd-Pd,bulk}$ = 2.0. N_{Au-Au} EXAFS fit of 9.3 was greater than $N_{Au-Au,bulk}$ and N_{Au-Pd} of 1.6 was less than $N_{Au-Pd,bulk}$. The Au EXAFS suggested there was some mixing of the Pd atoms with the Au; however, the core remained Au rich. By contrast, at the Pd edge, N_{Pd-Au} was equal to $N_{Pd-Au,bulk}$ and N_{Pd-Pd} was equal to $N_{Pd-Pd,bulk}$, suggesting that the NP surface underwent restructuring to give a composition similar to the bulk composition, i.e., a random and uniform composition (Fig. 5c). The difference in the state of Pd atoms before and after high-temperature treatment clearly showed the Pd atoms were located on the surface in the as-synthesized Pd/Au NPs [50,51]. On the other hand, hydrogen chemisorption and FT-IR spectroscopy with CO as the probe molecule [67,68] can indeed provide direct measurements of surface Pd atoms for comparison to EXAFS results. Such studies are currently underway.

3.3. TCE HDC catalytic activity comparison

Reaction rates of TCE HDC were determined as initial turnover frequency (TOF, mole of reacted TCE per surface Pd atom per second), with the implicit assumption of first-order dependence in TCE and zero-order in H_2 [50,51,69,70]. The kinetics is, in reality, more complicated at higher TCE concentrations for monometallic Pd catalysts [71]. Nevertheless, initial TOF's can be used to compare catalytic activities at a given TCE concentration and at an excess concentration of H_2. In accordance with our previous studies, Au NPs were found to be inactive, and the Pd-based NPs were active for the HDC reaction (Table 2). On the basis of an equal amount of surface Pd atoms charged to the batch reactor, the Pd/Au NPs were 10× more active than Pd NPs [51].

We performed TCE HDC reaction tests with colloidal NP suspensions for consistency with our previous works [50,51,54] rather than with immobilized NPs on carbon powders, which were used for XAS measurements. While the freeze-drying immobilization process is presumed to not affect NP structure due to its low temperature, the carbon support did influence the reaction kinetics due to loss of available active surface. In-depth analysis of NP/C catalysis and heat treatment effect on Pd-on-Au NP structure are underway.

Despite the inexact model (in which the TCE HDC reaction is presumed to be first-order in TCE concentration for all catalysts) used to quantify reaction rate, the large difference in values indicated a remarkably beneficial effect of Au on Pd activity. Observing that the TCE HDC activity (on a per-Pd-atom basis) increased with Pd surface coverage until it reached a maximum at 60–70% surface coverage, we had previously speculated that 2-dimensional Pd ensembles were formed at the lowest surface coverages before forming 3-dimensional Pd ensembles, which would have lowered Pd dispersion and therefore per-Pd-atom activity [51,52,54,72–74].

EXAFS analysis indicated the existence of monolayer-thin Pd clusters that were resistant to oxidation and mostly metallic under an ambient-temperature catalytic condition. We speculate that when Pd atoms are in contact with the metallic Au core, many, or perhaps all, of these remain metallic in air under conditions that the surface of Pd NPs is oxidized. Since the mild reaction conditions are insufficient to reduce these oxidized Pd, the Pd NP catalyst has low activity. We further speculate that higher Pd surface coverages in Pd/Au NPs lead to Pd multilayers, which easily get oxidized at an ambient temperature, contributing to lower activity at the higher surface coverages.

4. Conclusions

The bimetallic structure of Pd/Au NPs was characterized by TEM and XAS, and compared with Au NPs and Pd NPs. The Pd/Au NPs

were found to be consistent with a core–shell model in which Pd atoms were located on the surface of a Au-rich core. Whereas the Pd/Au NPs had nearly all its Pd atoms as surface atoms and only ~20% of these were oxidized, the monometallic Pd NPs had 25–35% of its Pd atoms as surface atoms and nearly all of these were oxidized. Since the oxidized surface of the monometallic Pd NPs is not reduced under the mild reaction conditions, the metallic Pd atoms of the Pd/Au NPs are suggested to be active sites for the room-temperature, water-phase reaction of TCE HDC. Heat treatment of carbon-supported NPs at 300 °C was sufficient to break apart the Pd-rich surface ensembles into a randomly distributed composition at the NP surface. Au NPs appear to have a unique ability to stabilize surface Pd atoms in metallic form, possibly leading to a set of highly active sites that is not present in monometallic Pd NPs under ambient-temperature reaction conditions.

Acknowledgments

This work is supported by the National Science Foundation (CBEN, EEC-0647452) and the Welch Foundation (C-1676). Materials Research Collaborative Access Team (MRCAT) operations (at the Advanced Photon Source, Argonne National Laboratory) are supported by the Department of Energy and the MRCAT member institutions. Use of the Advanced Photon Source is supported by the U. S. Department of Energy, Office of Science, and Office of Basic Energy Sciences, under Contract DE-AC02-06CH11357. We thank Dr. H.G. Bagaria (Rice University) for collecting TEM images and insightful discussions; Prof. J. Braam (Rice University) for use of the freeze-dryer and Mr. Y.-C. Tsai (Rice University) for assistance.

References

[1] N. Toshima, T. Yonezawa, New J. Chem. 22 (1998) 1179–1201.
[2] R. Ferrando, J. Jellinek, R.L. Johnston, Chem. Rev. 108 (2008) 845–910.
[3] D. Astruc (Ed.), Nanoparticles and Catalysis, Wiley, Weinheim, Germany, 2008.
[4] G. Schmid, A. Lehnert, J.O. Malm, J.O. Bovin, Angew. Chem. Int. Ed. Engl. 30 (1991) 874–876.
[5] A.M. Molenbroek, S. Haukka, B.S. Clausen, J. Phys. Chem. B 102 (1998) 10680–10689.
[6] A.E. Russell, A. Rose, Chem. Rev. 104 (2004) 4613–4635.
[7] C. Burda, X.B. Chen, R. Narayanan, M.A. El-Sayed, Chem. Rev. 105 (2005) 1025–1102.
[8] F. Maroun, F. Ozanam, O.M. Magnussen, R.J. Behm, Science 293 (2001) 1811–1814.
[9] R.J. Behm, Z. Phys. Chem.-Int. J. Res. Phys. Chem. Chem. Phys. 223 (2009) 9–36.
[10] V. Ponec, Appl. Catal. A: Gen. 222 (2001) 31–45.
[11] J.G. Chen, C.A. Menning, M.B. Zellner, Surf. Sci. Rep. 63 (2008) 201–254.
[12] M.S. Chen, D. Kumar, C.W. Yi, D.W. Goodman, Science 310 (2005) 291–293.
[13] T. Wei, J. Wang, D.W. Goodman, J. Phys. Chem. C 111 (2007) 8781–8788.
[14] B. Hammer, J.K. Norskov, Adv. Catal. 45 (2000) 71–129.
[15] J.R. Kitchin, J.K. Norskov, M.A. Barteau, J.G. Chen, Phys. Rev. Lett. 93 (2004).
[16] J.K. Norskov, T. Bligaard, J. Rossmeisl, C.H. Christensen, Nat. Chem. 1 (2009) 37–46.
[17] J.T. Miller, M.K. Neylon, C.L. Marshall, A.J. Kropf, in: C.I. Contescu, K. Putyera (Eds.), Dekker Encyclopedia of Nanoscience and Nanotechnology, CRC Press, Boca Raton, FL, 2004, pp. 3953–3972.
[18] G. Vlaic, D. Andreatta, P.E. Colavita, Catal. Today 41 (1998) 261–275.
[19] G. Meitzner, Catal. Today 39 (1998) 281–291.
[20] J.H. Sinfelt, J. Catal. 29 (1973) 308–315.
[21] J.H. Sinfelt, Acc. Chem. Res. 20 (1987) 134–139.
[22] G. Meitzner, G.H. Via, F.W. Lytle, J.H. Sinfelt, J. Chem. Phys. 78 (1983) 882–889.
[23] G. Meitzner, G.H. Via, F.W. Lytle, J.H. Sinfelt, J. Chem. Phys. 78 (1983) 2533–2541.
[24] G. Meitzner, G.H. Via, F.W. Lytle, J.H. Sinfelt, J. Chem. Phys. 83 (1985) 4793–4799.
[25] N. Toshima, M. Harada, T. Yonezawa, K. Kushihashi, K. Asakura, J. Phys. Chem. 95 (1991) 7448–7453.
[26] N. Toshima, M. Harada, Y. Yamazaki, K. Asakura, J. Phys. Chem. 96 (1992) 9927–9933.
[27] M. Harada, K. Asakura, Y. Ueki, N. Toshima, J. Phys. Chem. 96 (1992) 9730–9738.
[28] M. Harada, K. Asakura, N. Toshima, J. Phys. Chem. 97 (1993) 5103–5114.
[29] M. Harada, K. Asakura, N. Toshima, J. Phys. Chem. 98 (1994) 2653–2662.
[30] D.G. Duff, P.P. Edwards, J. Evans, J.T. Gauntlett, D.A. Jefferson, B.F.G. Johnson, A.I. Kirkland, D.J. Smith, Angew. Chem. Int. Ed. Engl. 28 (1989) 590–593.
[31] D. Richard, J.W. Couves, J.M. Thomas, Faraday Discuss. 92 (1991) 109–119.
[32] L.E. Aleandri, H. Bonnemann, D.J. Jones, J. Richter, J. Roziere, J. Mater. Chem. 5 (1995) 749–752.
[33] U. Kolb, S.A. Quaiser, M. Winter, M.T. Reetz, Chem. Mater. 8 (1996) 1889–1894.
[34] J.S. Bradley, G.H. Via, L. Bonneviot, E.W. Hill, Chem. Mater. 8 (1996) 1895–1903.
[35] A. Traverse, New J. Chem. 22 (1998) 677–683.
[36] A. Frenkel, Z. Kristallogr. 222 (2007) 605–611.
[37] S.N. Reifsnyder, H.H. Lamb, J. Phys. Chem. B 103 (1999) 321–329.
[38] C.R. Bian, S. Suzuki, K. Asakura, L. Ping, N. Toshima, J. Phys. Chem. B 106 (2002) 8587–8598.
[39] B.J. Hwang, L.S. Sarma, J.M. Chen, C.H. Chen, S.C. Shih, G.R. Wang, D.G. Liu, J.F. Lee, M.T. Tang, J. Am. Chem. Soc. 127 (2005) 11140–11145.
[40] M.R. Knecht, M.G. Weir, A.I. Frenkel, R.M. Crooks, Chem. Mater. 20 (2008) 1019–1028.
[41] S.M. Oxford, P.L. Lee, P.J. Chupas, K.W. Chapman, M.C. Kung, H.H. Kung, J. Phys. Chem. C (2010), doi:10.1021/jp103675n.
[42] R.J. Davis, M. Boudart, J. Phys. Chem. 98 (1994) 5471–5477.
[43] W.C. Ketchie, M. Murayama, R.J. Davis, J. Catal. 250 (2007) 264–273.
[44] C.H. Chen, L.S. Sarma, J.M. Chen, S.C. Shih, G.R. Wang, D.G. Liu, M.T. Tang, J.F. Lee, B.J. Hwang, ACS Nano 1 (2007) 114–125.
[45] P. Dash, T. Bond, C. Fowler, W. Hou, N. Coombs, R.W.J. Scott, J. Phys. Chem. C 113 (2009) 12719–12730.
[46] M.G. Weir, M.R. Knecht, A.I. Frenkel, R.M. Crooks, Langmuir 26 (2010) 1137–1146.
[47] K. Asakura, Y. Yamazaki, H. Kuroda, M. Harada, N. Toshima, Jpn. J. Appl. Phys. Part 1—Regul. Pap. Short Notes Rev. Pap. 32 (1993) 448–450.
[48] M. Harada, H. Einaga, J. Colloid Interface Sci. 308 (2007) 568–572.
[49] D. Ferrer, A. Torres-Castro, X. Gao, S. Sepulveda-Guzman, U. Ortiz-Mendez, M. Jose-Yacaman, Nano Lett. 7 (2007) 1701–1705.
[50] M.O. Nutt, J.B. Hughes, M.S. Wong, Environ. Sci. Technol. 39 (2005) 1346–1353.
[51] M.O. Nutt, K.N. Heck, P. Alvarez, M.S. Wong, Appl. Catal. B: Environ. 69 (2006) 115–125.
[52] M.S. Wong, P.J.J. Alvarez, Y.-L. Fang, N. Akçin, M.O. Nutt, J.T. Miller, K.N. Heck, J. Chem. Technol. Biotechnol. 84 (2009) 158–166.
[53] K.N. Heck, B.G. Janesko, G.E. Scuseria, N.J. Halas, M.S. Wong, J. Am. Chem. Soc. 130 (2008) 16592–16600.
[54] K.N. Heck, M.O. Nutt, P.J.J. Alvarez, M.S. Wong, J. Catal. 267 (2009) 97–104.
[55] L.N. Lewis, Chem. Rev. 93 (1993) 2693–2730.
[56] J.M. Thomas, Pure Appl. Chem. 60 (1988) 1517–1528.
[57] T. Teranishi, M. Miyake, Chem. Mater. 10 (1998) 594–600.
[58] D. Kashchiev, G.M. van Rosmalen, Cryst. Res. Technol. 38 (2003) 555–574.
[59] ImageJ, v. 1.40. National Institutes of Health, 2008 (http://rsb.info.nih.gov/ij/).
[60] T. Ressler, J. Synchrotron Radiat. 5 (1998) 118–122.
[61] F.W. Lytle, D.E. Sayers, E.A. Stern, Physica B 158 (1989) 701–722.
[62] G.H. Via, K.F. Drake, G. Meitzner, F.W. Lytle, J.H. Sinfelt, Catal. Lett. 5 (1990) 25–33.
[63] J.T. Miller, A.J. Kropf, Y. Zha, J.R. Regalbuto, L. Delannoy, C. Louis, E. Bus, J.A. van Bokhoven, J. Catal. 240 (2006) 222–234.
[64] D. Roth, P. Gelin, A. Kaddouri, E. Garbowski, M. Primet, E. Tena, Catal. Today 112 (2006) 134–138.
[65] P. Castellazzi, G. Groppi, P. Forzatti, A. Baylet, P. Marecot, D. Duprez, Catal. Today (2009), doi:10.1016/j.cattod. 2009.02.029.
[66] M.W. Tew, J.T. Miller, J.A. van Bokhoven, J. Phys. Chem. C 113 (2009) 15140–15147.
[67] H.G. Lang, S. Maldonado, K.J. Stevenson, B.D. Chandler, J. Am. Chem. Soc. 126 (2004) 12949–12956.
[68] J. Rebelli, M. Detwiler, S. Ma, C.T. Williams, J.R. Monnier, J. Catal. 270 (2010) 224–233.
[69] G.V. Lowry, M. Reinhard, Environ. Sci. Technol. 33 (1999) 1905–1910.
[70] F.D. Kopinke, K. Mackenzie, R. Kohler, Appl. Catal. B: Environ. 44 (2003) 15–24.
[71] Y.-L. Fang, K.N. Heck, P.J.J. Alvarez, M.S. Wong, in preparation.
[72] C.J. Baddeley, R.M. Ormerod, A.W. Stephenson, R.M. Lambert, J. Phys. Chem. 99 (1995) 5146–5151.
[73] A.W. Stephenson, C.J. Baddeley, M.S. Tikhov, R.M. Lambert, Surf. Sci. 398 (1998) 172–183.
[74] K.T. Park, K. Klier, C.B. Wang, W.X. Zhang, J. Phys. Chem. B 101 (1997) 5420–5428.